Investigation of impurity transport using supersonic molecular beam injected neon in HL-2A ECRH plasma*

Cui Xue-Wu(崔学武)†, Cui Zheng-Ying(崔正英), Feng Bei-Bin(冯北滨), Pan Yu-Dong(潘宇东), Zhou Hang-Yu(周航宇), Sun Ping(孙 平), Fu Bing-Zhong(傅炳忠), Lu Ping(卢 平), Dong Yun-Bo(董云波), Gao Jin-Ming(高金明), Song Shao-Dong(宋绍栋), and Yang Qing-Wei(杨青巍)

Southwestern Institute of Physics, Chengdu 610041, *China*

(Received 30 April 2013; revised manuscript received 8 June 2013)

In this paper, we describe the behavior of impurity transport in the HL-2A electron cyclotron resonance heating (ECRH) L-mode plasma. The neon as a trace impurity is injected by the supersonic molecular beam injection (SMBI) technique, which is used for the first time to study the impurity transport in HL-2A. The progression of neon ions is monitored by the soft X-ray camera and bolometer arrays with good temporal and spatial resolutions. The convection and diffusion process of the neon ions are investigated with the one-dimensional impurity transport code STRAHL. The results show that the diffusion coefficient D of neon ions is a factor of four larger than the neoclassical value in the central region. The value of D is larger in the outer region of the plasma ($\rho > 0.6$) than in the central region of the plasma ($\rho < 0.6$). The convective velocity directs inwards with a value of ~ -1.0 m/s in the Ohmic discharge, but it reverses to direct outwards with a value of ~ 8.0 m/s in the outer region of the plasma when ECRH is applied. The result indicates that the impurity transport is strongly enhanced with ECRH.

Keywords: impurity transport, impurity injection, SMBI, numerical simulation

PACS: 52.25.Vy, 52.25.Fi, 52.70.Kz **DOI:** 10.1088/1674-1056/22/12/125201

1. Introduction

Impurity transport in fusion devices plays a crucial role in plasma performances.[1] Impurities in the plasma core can enhance the radiation losses and affect the plasma stability. Especially, the discharge would be disrupted when the high Z impurity is accumulated in the plasma core. This would cause serious damage to the first wall of the fusion reactor. Testing the available theoretical predictions on the anomalous impurity transport is still one of the main tasks for experimental investigations. The behavior of impurity is exceedingly complex, because it is related to different impurity elements recycling from the complex geometry of the first wall of the device and also to the complicated atomic process. Understanding the impurity behavior in plasma, so as to be able to obtain effective methods of controlling impurity, is significant for fusion research and the realization of future reactors.

In general, transient perturbation methods are used to study impurity transport by injecting the trace impurity into tokamak plasma. The different impurity injection techniques have different injection efficiencies and therefore can play different roles in impurity transport study.[1] To develop a new method of injecting impurity is also very important, not only for the present tokamaks but also for the next experimental reactors like ITER. There are two commonly used techniques available in experiments: laser blow-off (LBO) for metal impurity injection and gas puff (GP) for gaseous impurity injection. The LBO technique is prevailing in the fusion research circle, but it usually injects one pulse in one discharge. There is an exception that in C-mod, two elements can be injected simultaneously in one discharge.[2] The injected impurities are also limited to the elements that can be coated on the films. The GP technique used in the impurity transport studies produces a source term whose duration is longer than the particle confinement time. This could affect the results of impurity transport analysis.

In the HL-2A tokamak, the supersonic molecular beam injection (SMBI) has been used for working gas fueling[3] on electron density feedback control. It is also frequently used for particle transport study[4] with the deep particle perturbation source and the well controlled particle quantity.[5] The molecular beam source can avoid some limitations of the periodic GP, such as the high particle recycling, the nonlinear edge process, and the rapid fall of the amplitude of the perturbation. On the other hand, the perturbation of the background plasma with the supersonic pulse injection can be limited to less than 5% in the electron density and temperature signals. The pulse duration is very short so that the parameters of the plasma would remain constant in the time interval of interest. This condition may not be achieved for the conventional gas puff because its perturbation to the background plasma could last several confinement times.[1] Therefore, it makes the supersonic pulsed injections very similar to the LBO injection in this respect. Furthermore, compared with the LBO, the su-

*Project supported by the National Natural Science Foundation of China (Grant Nos. 10975048, 11175061, and 10975049).

†Corresponding author. E-mail: cuixw@swip.ac.cn

© 2013 Chinese Physical Society and IOP Publishing Ltd

personic molecular beam injection cannot only inject the gas, such as neon, argon, etc., but also allow repeated injections in the same pulse (in principle, the number of injections is limited only by the plasma duration). This is an essential advantage to reduce the statistical uncertainties of the results without increasing the injected number of atoms above the trace level.[1]

The central electron cyclotron resonance heating (ECRH) could lead to a great reduction of the central impurity content since an increase of impurity diffusivity and a suppression of the convective pinch have been observed in the experiments. An outward impurity convection has also been reported.[6] The possible explanation of the increase of a positive (outward) convection in theoretical studies is that it is due to the density fluctuations caused by parallel compression,[7] but it is still not fully understood. Therefore, in this paper, the impurity transport study in ECRH discharges on HL-2A is conducted using the SMBI technique; the progression of impurity ions is monitored by the soft X-ray camera and bolometer arrays with good temporal and spatial resolutions.

The rest of this paper is organized as follows. The experimental conditions are described in Section 2 where the SMBI technique used for trace impurity injection is introduced. In Section 3, the experiments with neon injection into the ECRH plasma are conducted. The one-dimensional (1D) impurity transport simulation model is presented in Section 4. The simulation results and comparison between experiment and simulation are given in Section 5. The summary is contained in Section 6.

2. Experimental conditions and results

The HL-2A tokamak with two closed divertors was constructed in 2002. The designed parameters are as follows: major radius $R = 1.64$ m, minor radius $a = 0.4$ m, toroidal magnetic field $B_t = 2.8$ T, and plasma current $I_p = 480$ kA. The line averaged electron density is $n_e = 6 \times 10^{19}$ m^{-3} and the maximum electron temperature is $T_e = 5$ keV. It can be performed in the divertor and limiter configurations with similar plasma parameters.

The evolution of impurity ions in the main plasma is monitored by a 100-channel soft X-ray multi-camera system (five arrays, 20 channels for each array)[8] with the energy range of its detector being 1 keV–10 keV. The spatial and temporal resolutions of the system are 2.5 cm and 10 μs respectively. The time-dependent emission profiles of the injected impurity are derived from the local soft X-ray emissions. Meanwhile, the evolution of the total radiation loss is measured with multi-chord bolometric arrays (three arrays, 16 channels for each array). The time resolution is 50 μs and the spatial resolution is 2.5 cm. The line emission of neon at $\lambda = 1248$ Å is measured with a space-resolved 1-m normal incidence VUV spectrometer[9] working in a wavelength range of 300 Å–3200 Å and that at $\lambda = 416.2$ Å is measured with an EUV spectrometer working in a wavelength range of 30 Å–500 Å.[10] The source term in the simulation can be determined by these line emissions. The electron density profile is measured with an eight-chord HCN laser interferometer ($\lambda = 0.337$ mm) and the electron temperature profile is measured with electron cyclotron emission (ECE) diagnostic equipment with a spatial resolution of 2 cm and time resolution of 10 μs. The signal amplitude of the ECE diagnostic equipment is calibrated by the Thomson scattering measurement.

The experimental setup of the SMBI system in HL-2A and the structure of the molecular beam valve with cooling trap are shown in Fig. 1. The SMBI for plasma fueling consists of two lines: one injects gas from the high field side and the other is from the low field side, which is in the equatorial plane and perpendicular to the magnetic axis of the HL-2A torus. The latter is also used for impurity injection. Its valve with a 0.2-mm diameter cylinder can produce a gas beam with a higher speed and narrow angular distribution.[11] The distance between the nozzle of the valve and the last closed flux surface (LCFS) of the plasma is about 1.28 m. In order to maintain a good vacuum condition during the beam injection, a turbo-molecular pump with a pumping capacity of 450 l/s is installed in the injection tube. A tempered steel barrel 5-mm thick is used for shielding the valve against a stray magnetic field, which can disable the control of the valve. In this experiment, the number of injected molecular beam pulses can be adjusted from 10 to 15. The backing pressure of the pulsed solenoid valve is kept at a few 10^5 Pa. The pulse duration is usually set to be 5 ms.

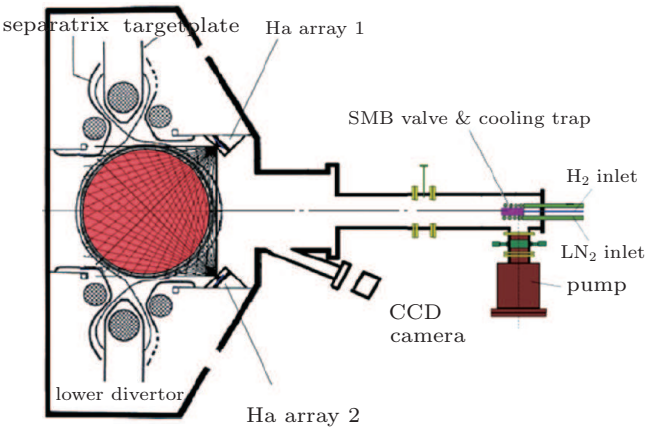


Fig. 1. (color online) Experimental setup of SMBI system in HL-2A tokamak.

A typical shot with six pulse injections of neon is shown in Fig. 2, where plasma current I_p, loop voltage V_l, line averaged electron density n_e, the soft X-ray signal, and bolometric signal are both at $\rho = 0.7$ and the SMBI signals are plotted from the top to the bottom. Here, ρ is the normalized poloidal flux coordinate. It clearly shows that the injection of neon does

not disturb the plasma parameters in any noticeable way based on the observations of I_p, V_l and n_e. By contrast, the features of the neon injection can be seen clearly from the soft X-ray signals and the bolometric signals. The time evolution of each pulse is nearly the same. Based on the analysis of each penetration process of neon ions, the transport coefficients of neon can be obtained. The uncertainties of the impurity transport coefficient can be reduced with a series of pulses. Furthermore, the multi-pulse injection can make feasible the study of impurity transport among different plasma regimes in one discharge. This can keep the least influences of the different discharge conditions, such as the wall recycling, on the impurity transport property. The experimental result demonstrates that the SMBI is suitable for impurity transport study.

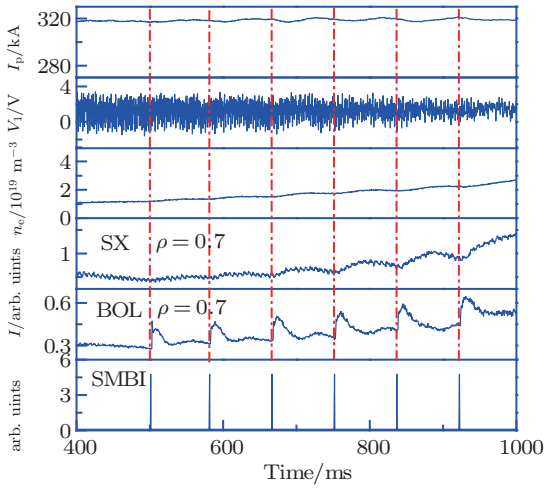


Fig. 2. (color online) Time evolutions for six neon pulses injected by SMBI, from the top to the bottom, are plasma current I_p, loop voltage V_l, line averaged electron density n_e, soft X-ray signal, and bolometric signal both at $\rho = 0.7$ and the SMBI signal in shot #15283.

3. Experimental results in ECRH plasma

In the HL-2A tokamak, the electron density usually decreases when the ECRH power is applied to the Ohmic discharges. This phenomenon is called "particle pump-out" and prevails in the ECRH L-mode plasma with a divertor configuration. The flattening of the impurity density profile is also frequently observed during the ECRH phase. In order to investigate the behaviors of impurity with ECRH, in particular the effect on its diffusion and convection, neon is injected into the ECRH phase using the SMBI technique. The experiment is carried out in discharge #19337, which is a typical shot with ECRH. It is shown in Fig. 3. The main parameters of the deuterium plasma are as follows: the plasma current $I_p = 170$ kA, the toroidal magnetic field $B_T = 1.23$ T, the line averaged electron density $n_e = 0.6 \times 10^{19}$ m^{-3}, and the ECRH heat power is stepped up in steps of 0.3 MW. One pulse of neon is injected at $t = 600$ ms right on the top of ECRH power of $P_{ECRH} = 1.5$ MW. It also indicates in Fig. 3 that the injection of neon does not disturb the main parameters of the plasma. The features of the neon injection are clear on the soft X-ray signals and the bolometric signals. The channels shown in Fig. 3 are $\rho = 0.2$ and $\rho = 0.7$ for soft X-ray signals and $\rho = 0.1$ and $\rho = 0.7$ for bolometric signals.

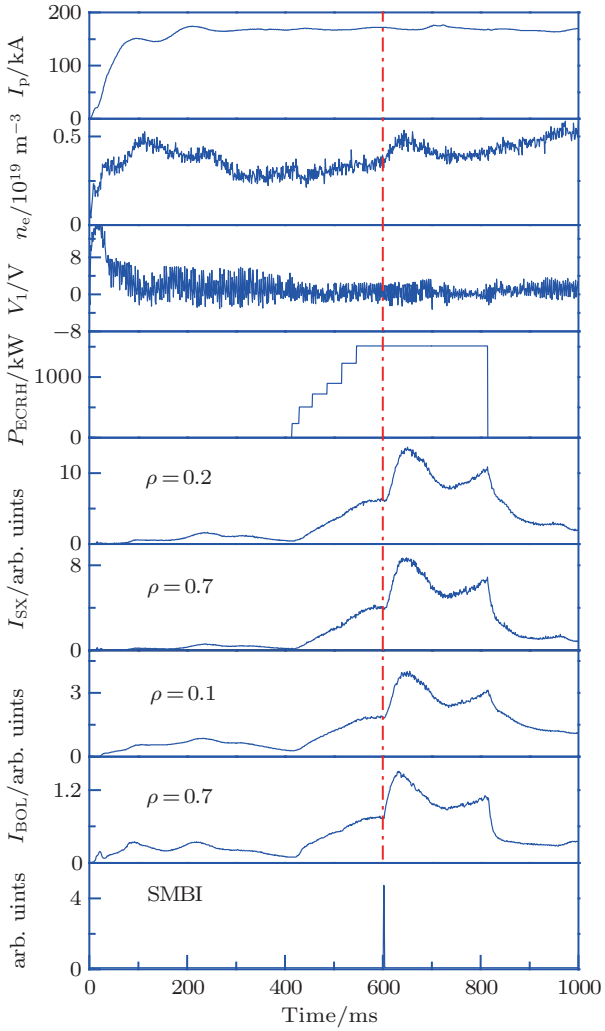


Fig. 3. (color online) Time evolutions for the neon injection with SMBI of plasma current I_p, loop voltage V_l, line averaged electron density n_e, ECRH heat power, soft X-ray signals at $\rho = 0.2$ and $\rho = 0.7$, the bolometric signals at $\rho = 0.1$, and $\rho = 0.7$ and the SMBI signal in shot #19337.

The expanded view of soft X-ray signals at the time of neon injection is presented in Fig. 4 with several channels. The contribution from the injected neon is taken into account. After the injection, the intensities of soft X-rays increase rapidly from the peripheral chords to the central chords; then they start to decrease. As the impurities propagate inwards, they enter into the regions with higher electron density and temperature. The intensities of the signals become strong. About 100 ms later, each signal decays to its pre-injection level. This indicates that the neon is not a re-cycling element.

As is well known, the dominant component of the soft X-ray is bremsstrahlung radiation, which is related to the effective ion charge, ion density of injected impurity, electron density, and temperature. In the injection process, the electron

density and temperature in the central region are not changed obviously after the injection. The density of injected impurity ions and the change of the effective charge Z make the most contributions to the change of the soft X-ray radiation. According to the corona equilibrium, the time scale of the ionization of the injected impurity is much shorter than the delay time of the peak of the soft X-ray signal. Therefore, the movements of the maximum radiation on the different channels of the soft X-ray from the outside region to the central region can approximately represent the transport behavior of the injected impurity. Figure 4 depicts the position of the maximum radiation on each channel. It shows that the increased ramping rate of the soft X-ray intensity in the edge region of the plasma is obviously greater than that in the center. It takes about 30 ms to reach its peak for the edge channel at $r = 26.9$ cm but it spends about 50 ms for the central channel at $r = 2.5$ cm. This implies that the transport of impurities is much slower in the central region of the plasma than in the outer part of the plasma. There are obviously two regimes with different velocities. The inward speed of the impurity can be approximately calculated by the movement of the maximum radiation of different channels. The more accurate calculations of the impurity transport coefficients are obtained by the numerical simulation code.

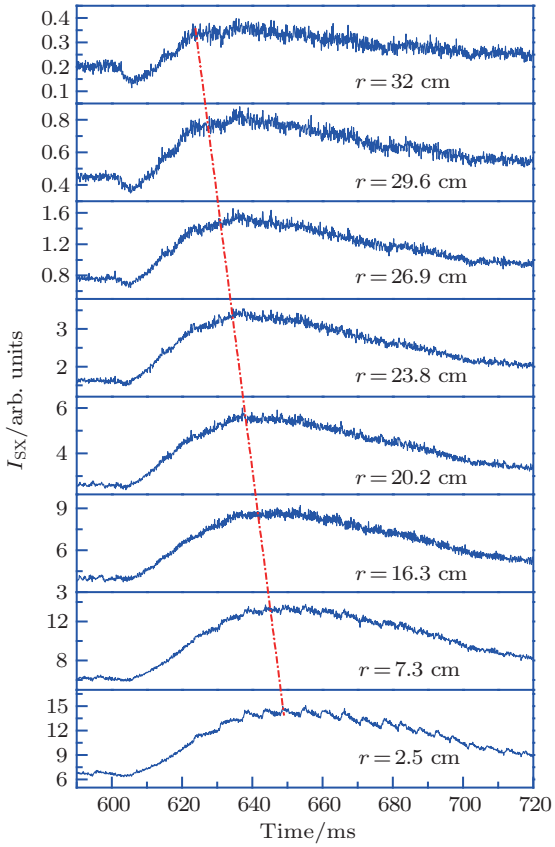


Fig. 4. (color online) Time evolutions of the expanded view of soft X-ray emission for several chords in the HL-2A shot #19337.

After the soft X-ray emission arrives at a maximum, the intensity decreases exponentially. The radiation during this period can be expressed by the formula $I = I_0 \mathrm{e}^{-t/\tau_p}$. This characteristic time τ_p is explained as the global particle confinement time for the non-recycling injected trace impurities. Fits are typically taken between the times when the signal has fallen from 80% to 10% of the peak value. By fitting the central chord $r = 2.5$ cm soft X-ray signal, the particle confinement time is obtained to be 60 ms. The τ_p at the edge channel $r = 26.9$ cm is about 40 ms. This suggests that the transport of impurities is slower in the central region of the plasma than in the outer part of it.

In the expanded view of the central channel signal shown in Fig. 5, the sawteeth are inverted. There are also some small inverted sawteeth before the impurity injection; however, the sawteeth are also inverted after the impurity injection in the rising phase or in the decreasing phase. The only difference is that the amplitudes of the inverted sawteeth are amplified during the impurity injection. At the rising phase, a jump with a period of about 350 μs is clearly shown during the inverted sawteeth's crashing. This implies that the inward flow of impurities is enhanced when the sawteeth crash.

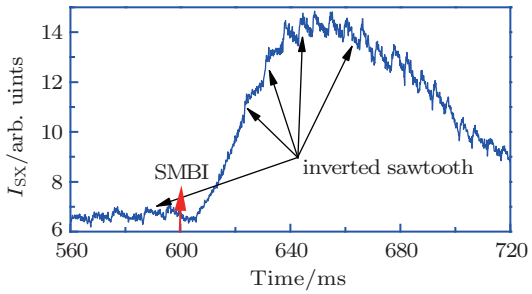


Fig. 5. (color online) Time evolution of the local soft X-ray signal I_{SX} at $r = 2.5$ cm for HL-2A shot #19337.

4. Transport simulations model

The local transport analysis is performed using the impurity radial transport code STRAHL.[12] The continuity equations are solved for all the ionization stages of the injected element over the time interval when the injected impurity is present in the plasma core. The continuity equation is expressed as

$$\frac{\partial n_Z}{\partial t} + \nabla \cdot \Gamma_Z = S_{Z-1} + R_{Z+1} - (S_Z + R_Z) + S_q, \qquad (1)$$

where the subscript Z denotes the charge of the ionization stage, n_Z is the impurity density in ionization state Z, Γ_Z is the impurity flux density, S_Z and R_Z are the ionization and recombination terms respectively and S_q is the external source. The last item on the right-hand side in Eq. (1) comprises the gas injection for the neutral state and losses in the scrape-off

layer for all states. The impurity radial flux is assumed to be the sum of a diffusive term and a convective term:

$$\Gamma_Z(r) = -D(r)\nabla n_Z(r) + V(r)n_Z(r), \tag{2}$$

where $D(r)$ is the diffusion coefficient and $V(r)$ the convective velocity. The $D(r)$ and $V(r)$ coefficients are assumed to be time-independent since the background plasma is almost constant and the injected impurity is a trace. The 1D nature of the STRAHL code imposes the hypothesis of toroidal and poloidal symmetries.

A separate equation is included to describe the ionization of the injected neutral atoms of density n_0. The boundary condition for this equation at the last mesh radius $r = a$ is written as

$$\Gamma_0 = n_0(a)V_0 = \Gamma_{\rm ext} + R\sum_Z \Gamma_Z(a). \tag{3}$$

Thus, Γ_0, the total neutral particle flux density entering into the plasma with a directed velocity V_0, is set to be the sum of an external flux density $\Gamma_{\rm ext}$, and a recycling flux density. The latter is the total outward flux density $\sum_Z \Gamma_Z(a)$ at the last mesh, recycled with a recycling coefficient R. The radial flux density Γ_Z is described using Eq. (2).

The energy losses due to impurities are composed of ionization, line radiation, recombination, and bremsstrahlung for tokamak plasma. The corresponding power densities of these four kinds of emissions are listed below (all in unit of W·m^{-3})

$$P_i = c_1 \sum_{Z=1}^{M-1} n_{\rm e} n_Z \alpha_Z \left(\chi_Z + \frac{3}{2}T_{\rm e}\right) + P_{\rm rec}, \tag{4}$$

$$P_{\rm rec} = c_2 \sum_{Z=1}^{M-1} \left(\frac{3}{2} n_{\rm e} n_{Z+1} \beta_Z T_{\rm e}\right), \tag{5}$$

$$P_{\rm br} = c_3 Z_{\rm eff} n_{\rm e}^2 T_{\rm e}^{1/2}, \tag{6}$$

$$P_{\rm ex} = c_4 n_{\rm e} T_{\rm e}^{-1/2} \sum_{Z=2}^{M-1} n_Z \sum_{l=1}^{L} c_{Zl} \exp\left(-\frac{\chi_{\rm ex}}{T_{\rm e}}\right), \tag{7}$$

where M is the atomic number, χ_Z is the ionization energy, $Z_{\rm eff}$ is the effective ionic charge, $\chi_{\rm ex}$ is the excitation energy, c_1–c_4 are the constants, and $C_{Zl} = \overline{\Omega}B/\omega(\chi_{\rm ex}/\chi_{\rm h})$, with $\overline{\Omega}$ being the effective collision strength, ω the statistical weight, B the branching ratio, and $\chi_{\rm h}$ the ionization potentials of hydrogen.[13]

The main input data to the code are the external source term, the electron density and temperature profiles of plasma over the time interval of interest. The STRAHL code starts from an initial guess of the transport coefficient radial profiles. After solving the coupled continuity equations, the STRAHL reconstructs the EUV and VUV line emissions, bolometric and soft X-ray brightness. Then the transport coefficient profiles are modified iteratively until the difference between the reconstructed signals and the measured ones is minimized in a least squares (χ^2) sense. Finally, a successful model for the impurity transport is produced. In this way, the transport coefficients of impurities, each as a function of the radius, are acquired.

5. Simulation results

The transport coefficients of impurities, including diffusion coefficient $D(r)$ and convective velocity $V(r)$, are derived using the impurity transport code STRAHL. The brightness of soft X-ray signal $E_{\rm SX}$ (normalized) and total radiation losses $E_{\rm BOL}$ (normalized) are used for the simulation and the results are shown in Fig. 6. The background radiation before SMBI has been subtracted. Since the particle confinement time $\tau_{\rm p}$ is about 40 ms, the time interval of interest on the signals is limited to $t = 700$ ms. The solid lines and the dotted lines denote the experimental and simulation result, respectively. In this figure, five channels of soft X-ray signals are presented in Figs. 6(a) to 6(e) and four channels of bolometric signals are shown in Figs. 6(f) to 6(i). The results show that the agreement between the simulation and experiment is good. That means that the obtained transport coefficients can explain the impurity transport feature of this ECRH L-mode discharge very well.

The obtained transport coefficients for the good fitting of the experimental results are shown by the diffusion coefficient profile (DP) #2 and the convective velocity profile (VP) #2 in Figs. 7(a) and 7(b) by the dotted lines with open circles, respectively. The corresponding values of the diffusion coefficient $D(r)$ are 0.2, 0.3, 0.45, 0.8 and 1.0 m^2/s at $\rho = 0$, 0.68, 0.7, 0.72, and 0.9 respectively. The neoclassical transport coefficients are also calculated using the neoclassical transport equations.[14] The neoclassical diffusion coefficient is less than 0.05 m^2/s in the plasma center and 0.1 m^2/s at the plasma edge. This indicates that the transport of impurity in the ECRH L-mode plasma is anomalous. At present, the transport parameters beyond $\rho = 0.9$ are inaccurate, because the complex processes in the scrap-off-layer (SOL) are not considered in detail in the code. In Fig. 7(b), the convective velocity $V(r)$ of #2 is negative at the central region and positive in the outer region of the plasma. The relevant values of $V(r)$ are -0.9, -1 and -0.6 m/s at $\rho = 0.25$, 0.32, and 0.53 respectively and $V = 1$, 6, and 8 m/s at $\rho = 0.63$, 0.71 and 0.8 respectively. This implies that the convective velocity directs inwards in the central region ($\rho < 0.6$) but it reverses to direct outwards in the outer region of the plasma ($\rho > 0.6$) when ECRH is applied. The result indicates that the impurity transport is strongly enhanced with ECRH, especially in the outer region of the plasma.

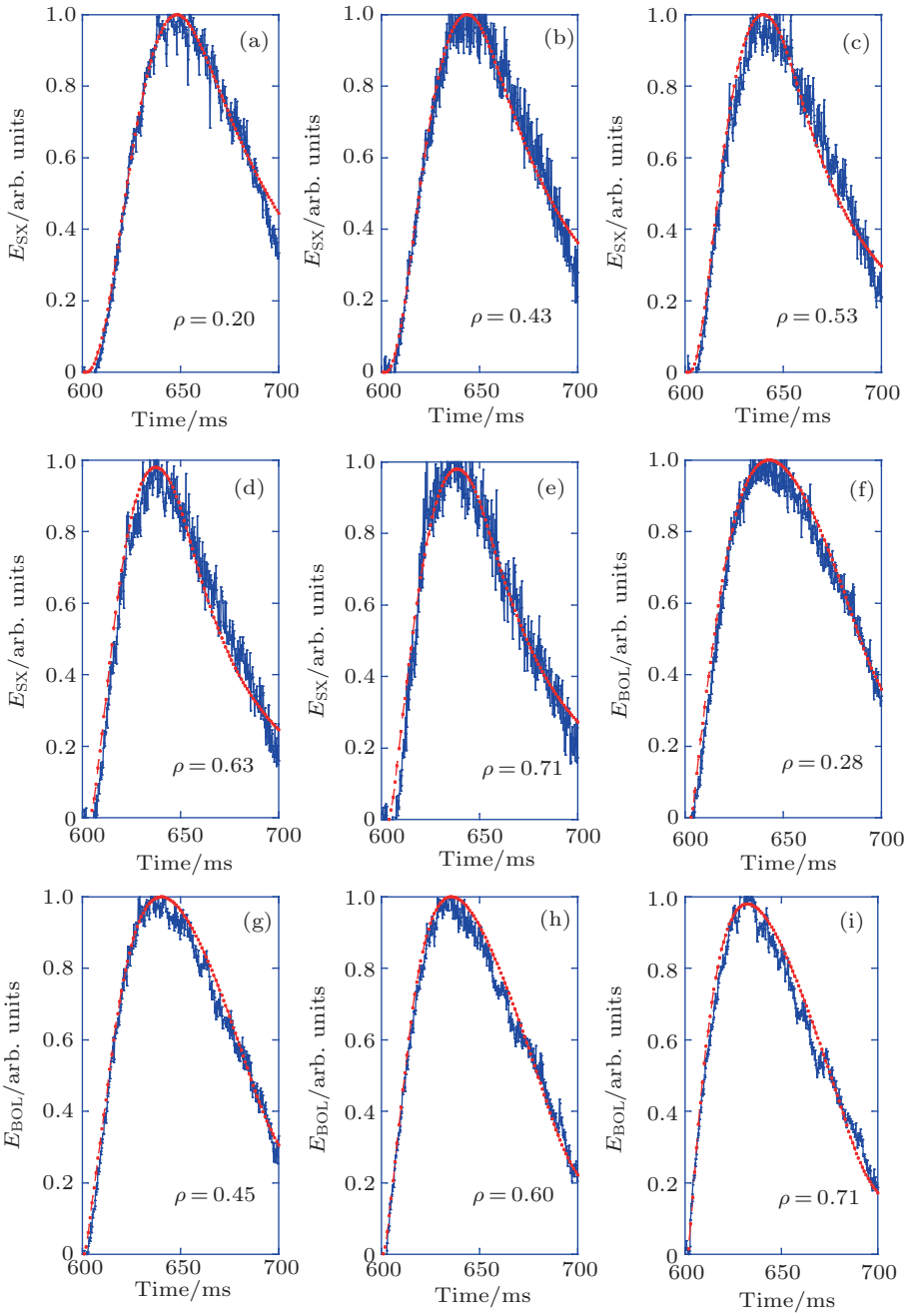


Fig. 6. (color online) (a)–(e) Time evolutions of the soft X-ray brightness and (f)–(i) total radiation losses for the HL-2A shot #19337 (solid lines). The background radiation before SMBI has been subtracted. The simulated curves (dotted lines) are also shown.

It is difficult to estimate the uncertainties of the obtained transport coefficients accurately. Therefore, the validity of the impurity transport coefficients shown in Fig. 7 by the profiles #2 is simply assessed as follows. The simulations are also performed by varying the diffusion coefficient and convective velocity, respectively. Since the uncertainties of the obtained transport coefficients are mostly caused by the error bar of the measured data. The calculated total radiation losses with different profiles of convective velocity are compared with the measured results with their measurement errors. The results are shown in Fig. 8 where the total radiation losses for two typical channels in the core region at $\rho = 0.28$ and in the outer region at $\rho = 0.71$ of the plasma are presented respectively. The diffusion coefficient D is fixed as the DP #2 in Fig. 7(a). In addition to VP #2, which gives the best fitting in the χ^2 sense of the experiments, another three profiles of the convective velocity are plotted in Fig. 7(b). The values of V in the core region of $\rho < 0.6$ are set to be the same as that of VP #2, while the values of V are set to be 15 m/s, 2 m/s, and -2 m/s at $\rho = 1$ for VP #1, #3, and #4, respectively. In order to show an obvious difference between the calculation and the experiment, the large changes of V are adopted.

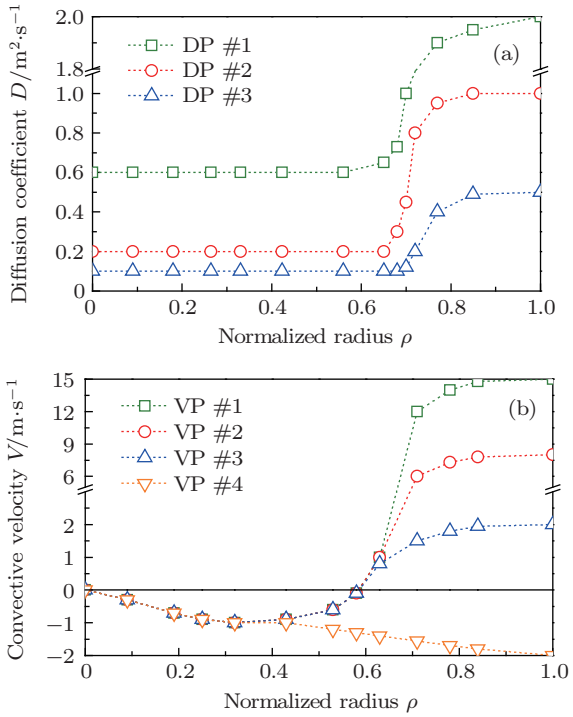


Fig. 7. (color online) Profiles of (a) diffusion coefficient D and (b) convective velocity V for the HL-2A shot #19337.

From Fig. 8(a) for the core and Fig. 8(b) for the outer regions of plasma, it follows that the increase and the decrease of the calculated bolometric signals during the rising phase and the decay phase, respectively, become slow when the convective velocity changes from VP #1 (positive) to VP #4 (negative). Especially, the larger the positive convective velocities at $\rho = 1$, the more rapidly the bolometric signals increase in the rising phase and decrease in the decay phase. This is mainly caused by the enhancement of impurity transport with the outward convective velocity. On the other hand, the relative good particle confinement could be achieved when V is set to be in the inward direction. From Fig. 8, it is clearly seen that the convective velocity should be less than 15 m/s and larger than 2 m/s. Since the measurement errors of the bolometric signals in HL-2A are about 5%, the convection velocity may be modified as $V(\rho = 1) = (8 \pm 2)$ m/s. Therefore, the convection velocity profile VP #2 may be given by $V(\rho = 1) = 8$ m/s with 25% error, which is appropriate in the χ^2 sense.

The error bar of the obtained diffusion coefficient is estimated in the same way as that mentioned above. In Fig. 9, the time evolutions of the total radiation losses obtained from the experiments are compared with the simulations for different values of diffusion coefficient D for two typical channels in the core region ($\rho = 0.28$) and in the outer region ($\rho = 0.71$) ofthe plasma, respectively. The convective velocity is fixed as VP #2, shown in Fig. 7(b). There are shown two profiles of the diffusion coefficient, i.e., #1 and #3 in addition to DP #2 in Fig. 7(a). One is $D(\rho < 0.6) = 0.6$ m^2/s and $D(\rho > 0.6) = 2$ m^2/s, as shown by DP #1. The other is $D(\rho < 0.6) = 0.1$ m^2/s and $D(\rho > 0.6) = 0.5$ m^2/s, as marked by DP #3. The results shown in Fig. 9 indicate that the influence of the diffusion coefficient D on the calculated bolometric signals is not so significant as that of the convective velocities. However, the effects are still obvious.

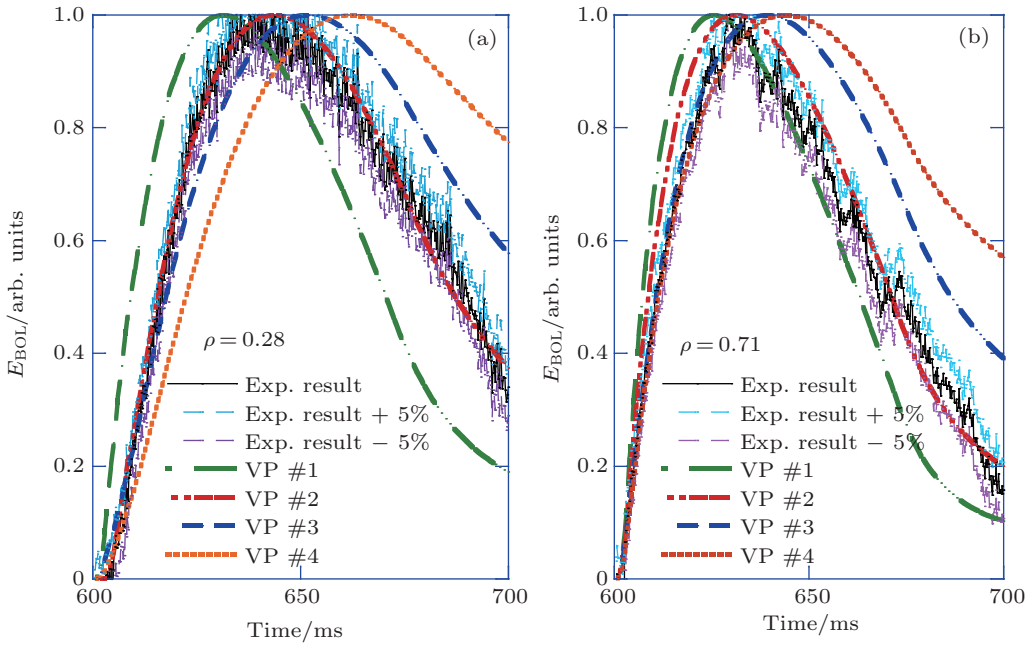


Fig. 8. (color online) Time evolutions of the total radiation losses for (a) $p = 0.28$ and (b) $p = 0.71$, showing the comparison between the measurements and the simulations for different convective velocities.

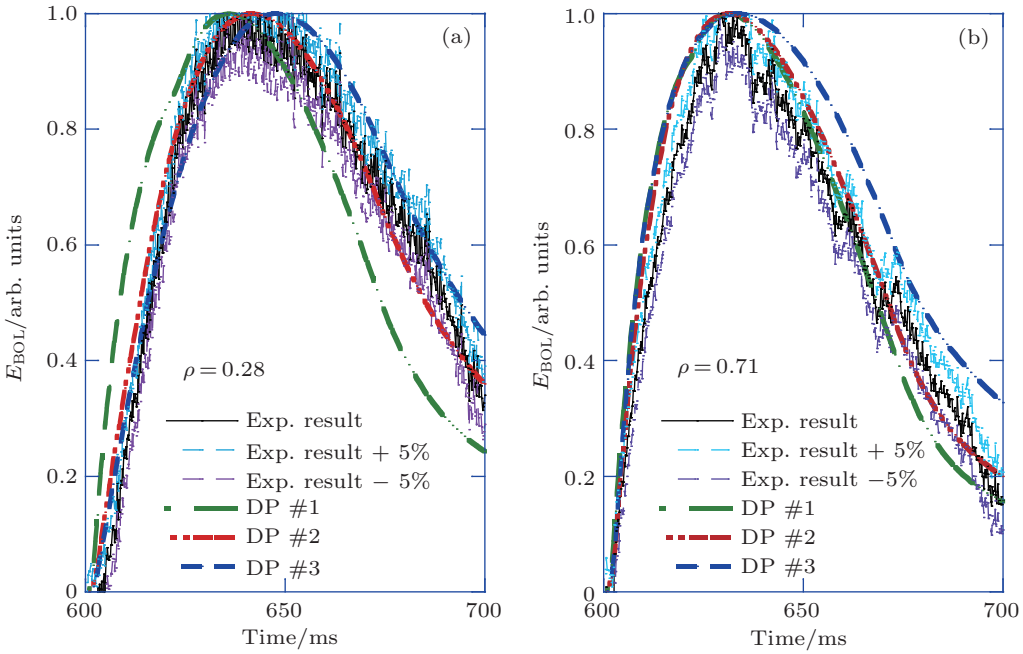


Fig. 9. (color online) Time evolutions of the total radiation losses for (a) $p = 0.28$ and (b) $p = 0.71$, showing the comparison between the measurements and the simulations for different diffusion coefficients.

From Fig. 9(a) for the core and Fig. 9(b) for the outer regions, it can be seen that the bolometric signals calculated with DP #1 increase rapidly in the rising phase and decrease rapidly in the decay phase compared with the measured one. Meanwhile, the bolometric signals behave a little slowly in both the rising and the decay phases for the DP #3. Therefore, a good agreement between experiment and calculation can be obtained for 0.1 m^2/s $< D(\rho < 0.6) <$ 0.6 m^2/s in the central region and 0.5 m^2/s $< D(\rho > 0.6) <$ 2 m^2/s for the outer region, which are shown in Fig. 9. Considering the measurement errors of the bolometric signals (about 5%), a good fitting of the experiments could be obtained with the values of the diffusion coefficient of $D(\rho < 0.6) = (0.2 \pm 0.1)$ m^2/s and $D(\rho > 0.6) = (1 \pm 0.4)$ m^2/s. Therefore, the maximum error of the diffusion coefficient is estimated to be about 40%. The profile of $D(\rho < 0.6) = 0.2$ m^2/s and $D(\rho > 0.6) = 1$ m^2/s, is appropriate in the χ^2 sense for obtaining the best fittings of the measured signals.

From the above discussion, the suitable transport coefficients for the present ECRH L-mode plasma are $D(\rho > 0.6) =$ 1 m^2/s and $V(\rho > 0.6) = 8$ m/s. This result suggests that an outward flux of impurity can be expected when the ECRH power is injected, which means that the impurity content in the plasma core can be controlled with the central ECRH power. The result presented here is also in good agreement with the previous observation in which the convective velocity of carbon impurity directs outwards with a value of 7 m/s in the outer region of HL-2A plasma operating with ECRH.[15]

6. Summary

The experimental results demonstrate that the supersonic molecular beam injection (SMBI) is suitable for impurity transport study. Not only can it avoid some of the limitations of the periodic GP, but also the perturbation of the background plasma with the supersonic pulse injection is extremely small and the pulse duration is very short. In this paper, neon serving as a trace impurity is successfully injected by this technique, which is adopted for the first time for the impurity transport study in HL-2A. The transport of neon is studied in the HL-2A ECRH L-mode plasma. The dedicated diagnostics for this study are a soft X-ray camera and bolometer arrays. After neon is injected, it is found, using the soft X-ray cameras experimentally, that the injected impurities first go inward and then diffuse out. By fitting the central chord of the soft X-ray signal in the decay phase, the particle confinement time is given by 60 ms. Meanwhile, the particle confinement time at $r = 26.9$ cm is about 40 ms. This suggests that the transport of impurities is slower in the central region than in the outer region of the plasma.

The diffusion coefficient D and convective velocity V determined using the impurity transport code STRAHL are compared with those measured by the soft X-ray camera and bolometer arrays for the HL-2A ECRH discharges. In the central region of plasma $0 \leq \rho \leq 0.6$, the typical values of diffusion coefficient D and convective velocity V are about 0.2 m^2/s and -1.0 m/s, respectively. In the outer part of plasma $0.6 \leq \rho \leq 1$, the values of diffusion coefficient D and convective coefficient V increase to 1.0 m^2/s and 8 m/s in this discharge. They are much larger than the neoclassical values.

This indicates that the transport of impurity is anomalous and an outward impurity flux is obtained when the ECRH power is applied. The study of the physics mechanism behind the reversal of the convective velocity of impurity directing outward in the outer region of plasma operating with ECRH will be carried in the HL-2A tokamak theoretically and experimentally.

Acknowledgments

The authors would like to thank Dr. R. Dux from IPP for making a great effort to transfer the STRAHL code to SWIP, Prof. S. Morita and Dr. M. Goto from NIFS for supplying the development of the vacuum ultraviolet (VUV) and extreme ultraviolet (EUV) spectrometers in HL-2A. The authors also thank the HL-2A team for their contributions to the HL-2A operation.

References

[1] Guirlt R, Villegas D, Parisot T, Bourdelle C, Garbet X, Imbeaux F, Mazon D and Pacella D 2009 *Nucl. Fusion* **49** 055007

[2] Howard N T, Greenwald M and Rice J E 2011 *Rev. Sci. Instrum.* **82** 0335

[3] Yao L H, Feng B B, Chen C Y, Shi Z B, Yuan B S, Zhou Y, Duan X R, Sun H J, Lu J, Jiao Y M, Ni G Q, Lu H Y, Xiao W W, Li W, Pan Y D, Hong W Y, Ran H, Ding X T and Liu Y 2007 *Nucl. Fusion* **47** 1399

[4] Xiao W W, Zhou X L, Ding X T, Yao L H, Feng B B, Song X M, Song S D, Zhou Y, Liu Z T, Yuan B S, Sun H J, Ji X Q, Gao Y D, Li Y G, Yan L W, Yang Q W, Liu Y, Dong J Q, Duan X R, Liu Y, Pan C H and HL-2A Team 2010 *Phys. Rev. Lett.* **104** 215001

[5] Ding X T, Zhou Y, Deng Z C, Xiao W W, Liu Z T, Shi Z B, Yan L W, Hong W Y and Yang Q W 2006 *Rev. Sci. Instrum.* **77** 10F528

[6] Sertoli M, Angioni C, Dux R, Putterich T, Igochine V and ASDEX Upgrade Team 2011 *Plasma Phys. Control Fusion* **53** 035024

[7] Angioni C and Peeters A G 2006 *Phys. Rev. Lett.* **96** 095003

[8] Liu Y, Peterson B J, Dong Y B, Pan Y D and Deng W 2006 *Plasma Sci. Technol.* **8** 41

[9] Cui Z Y, Morita S, Fu B Z, Huang Y, Sun P, Gao Y D, Xu Y, Dong C F, Lu P, Wang Q M, Ding X T, Yang Q W and Duan X R 2010 *Rev. Sci. Instrum.* **81** 043503

[10] Zhou H Y, Cui Z Y, Morita S, Fu B Z, Goto M, Sun P, Dong C F, Gao Y D, Xu Y, Lu P, Yang Q W and Duan X R 2012 *Rev. Sci. Instrum.* **83** 10D507

[11] Yao L H, Zhou Y, Cao J Y, Feng B B, Feng Z, Luo J L, Dong J F, Yan L W, Hong W Y, Li K H, Cui Z Y, Liu Y, Wang E Y, Yan J C and HL-1M Team 2001 *Nucl. Fusion* **41** 817

[12] Behringer K 1987 Jet Report JET-R (87) 08

[13] Tazima T, Nakamura Y and Inoue K 1977 *Nucl. Fusion* **17** 419

[14] Fussmann G, Field A R, Kallenbach K, Steuer K H and The ASDEX Upgrade Team 1991 *Plasma Phys. Control Fusion* **13** 1677

[15] Cui Z Y, Morita S, Zhou H Y, Ding X T, Sun P, Kobayashi M, Cui X W, Xu Y, Huang X L, Shi Z B, Cheng J, Li Y G, Feng B B, Song S D, Yan L W, Yang Q W and Duan X R 2013 *Nucl. Fusion* **53** 093001